

Transport Theory of Half-quantized Hall Conductance in a Semi-magnetic Topological Insulator

Humian Zhou,¹ Hailong Li,¹ Dong-Hui Xu,² Chui-Zhen Chen,^{3,4,*} Qing-Feng Sun,^{1,5,6} and X. C. Xie^{1,5,6,†}

¹*International Center for Quantum Materials, School of Physics, Peking University, Beijing 100871, China*

²*Department of Physics, Chongqing University, Chongqing 400044, China*

³*School of Physical Science and Technology, Soochow University, Suzhou 215006, China*

⁴*Institute for Advanced Study, Soochow University, Suzhou 215006, China*

⁵*Collaborative Innovation Center of Quantum Matter, Beijing 100871, China*

⁶*CAS Center for Excellence in Topological Quantum Computation, University of Chinese Academy of Sciences, Beijing 100190, China*

Recently, a half-quantized Hall conductance (HQHC) plateau is experimentally observed in a semi-magnetic topological insulator heterostructure. However, the heterostructure is metallic with a nonzero longitudinal conductance, which contradicts the common belief that quantized Hall conductance is usually observed in insulators. In this work, we systematically study the surface transport of the semi-magnetic topological insulator with both gapped and gapless Dirac surfaces in the presence of dephasing process. In particular, we reveal that the HQHC is directly related to the half-quantized chiral current along the edge of a strongly dephasing metal. The Hall conductance keeps a half-quantized value for large dephasing strengths, while the longitudinal conductance varies with Fermi energies and dephasing strengths. Furthermore, we evaluate both the conductance and resistance as a function of the temperature, which is consistent with the experimental results. Our results not only provide the microscopic transport mechanism of the HQHC, but also are instructive for the probe of the HQHC in future experiments.

PACS numbers:

Keywords:

Introduction.— The investigation of the Dirac fermions is an important paradigm in modern condensed matter physics [1–9]. Fundamentally, a single two-dimensional (2D) massive Dirac cone exhibits a hallmark half-quantized Hall conductance (HQHC) [1–3], which plays an essential role in formulating various topological effects [10–12]. Typical examples of this include quantum anomalous Hall (QAH) effect proposed by Haldane, topological magnetoelectric effect in axion insulators and topological valley currents in 2D materials [5, 10–12]. So far, many theoretical and experimental efforts have been exerted to observe the HQHC, but the direct observation of the HQHC remains elusive [13–20]. First, that’s because the Dirac fermions of opposite chirality always appear in pairs in realistic systems according to fermion doubling theory [21]. More importantly, unlike the integer QAH effect that supports dissipationless chiral edge modes, a single 2D massive Dirac cone does not possess topologically protected edge states and thus the mechanism of the HQHC goes beyond conventional paradigm of quantized transport.

Very recently, a breakthrough is made to the experimental observation of the HQHC in a semi-magnetic topological insulator (TI) heterostructure [22]. The semi-magnetic TI heterostructure consists of a single massive Dirac cone on the top surface and a massless Dirac cone on the bottom surface [see Fig. 1(a)] and thus it manifests as a metal in the transport measurement. It is found that the Hall and longitudinal resistance that directly measured in the experiment are non-quantized. Surpris-

ingly, by converting the resistance into the conductance, the Hall conductance is half-quantized in such a metallic phase, where the longitudinal conductance is nonzero. This is in stark contrast to the common belief that quantized Hall conductance is generally observed in an insulating phase such as the QAH effect [5]. Until now, the microscopic mechanism for the HQHC in such a metallic heterostructure is unclear.

In this Letter, we uncover that the HQHC originates from a half-quantized chiral current propagating along the edge of a strongly dephasing metal, which we called classical metal. To be specific, we study the surface transport of the semi-magnetic TI in the presence of dephasing process by Landauer-Büttiker formula. It is found that the the Hall conductance σ_{xy} arrives at a half-quantized plateau when dephasing strength exceeds a critical value, whereas the longitudinal conductance σ_{xx} is nonzero. Further, we show that the difference of transmission coefficients t_d along the edge of the sample is half-quantized and independent of dephasing strength, giving rise to a robust half-quantized chiral edge current. Then, by establishing an analytic relation between σ_{xy} and t_d , we reveal that the half-quantized t_d can lead to the HQHC in the classical metal limit, where the system size is much larger than the phase coherent length. To compare with the experimental results [22], we calculate the Hall and longitudinal conductance at low temperature. It is show that σ_{xy} remains half-quantized regardless of temperature while σ_{xx} monotonically increases with the temperature, which is consistent with the experimental results.

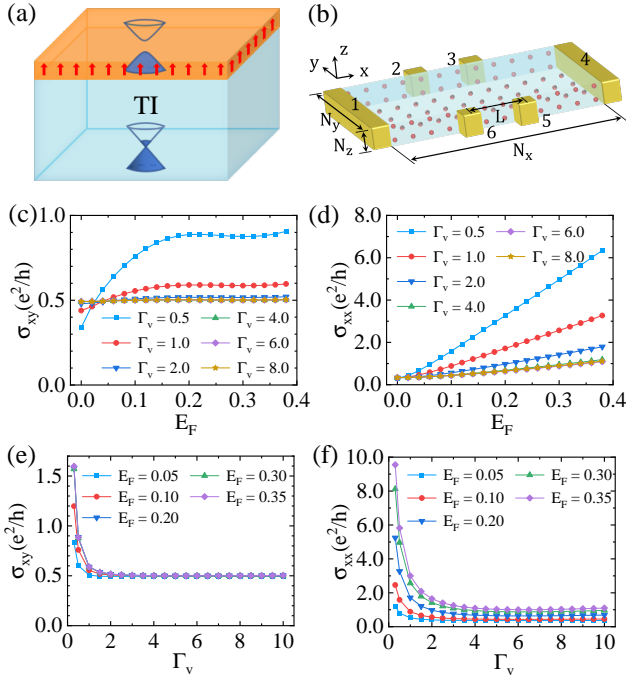


FIG. 1: (Color online). (a) Schematic plot of a semi-magnetic TI with a gapped Dirac cone on the top surface and a gapless Dirac cone on the bottom surface, where the red arrows indicate the magnetization on the top surface. (b) Schematic plot of a six-terminal Hall-bar device, where the red balls represent the sites attached virtual leads. The distance of two nearest balls is 4. (c) and (d) illustrate the Hall conductance σ_{xy} and the longitudinal conductance σ_{xx} against Fermi energy E_F for different dephasing strengths Γ_v , respectively. (e) and (f) illustrate σ_{xy} and σ_{xx} against Γ_v for different E_F , respectively. Here, $N_x = 640$, $N_y = 153$, $N_z = 5$, $n_x = 160$, $n_y = 39$, $n_z = 2$, and the distance between lead 5 and 6 is $L = 40$. The model parameters are fixed as $A = 1.0$, $B = 0.6$, $M_0 = 1.0$ and $M_z = 0.4$.

Model Hamiltonian and dephasing.—We consider a semi-magnetic TI heterostructure shown in Fig. 1(a). The four-band effective Hamiltonian is $H = H_0 + H_M$, where

$$H_0(\mathbf{k}) = \sum_{i=x,y,z} Ak_i \sigma_x \otimes s_i + (M_0 - Bk^2) \sigma_z \otimes s_0$$

describes the isotropic 3D TI [6], with model parameters A , B , and M_0 . σ_i and s_i are Pauli matrices for the orbital and spin degrees of freedom, respectively. $H_M = M(z)\sigma_0 \otimes s_z$ is the Zeeman splitting, where $M(z)$ takes the value M_z on the top surface, and zero elsewhere. When $0 < M_0 < 4B$, the 3D TI material is topologically nontrivial, and then it has a single gapless Dirac cone on each surface. Due to the Zeeman splitting H_M , an Dirac gap $\Delta = 2M_z$ is opened up on the top surface, giving rise to a gapped Dirac cone with the HQHC. Therefore, the semi-magnetic TI hosts a gapped Dirac cone and a gapless Dirac cone on the top and bottom surfaces, re-

spectively [see Fig. 1(a)]. Note that numerical results, calculated by using a real-space Kubo formula [23, 24], demonstrate that the Hall conductance from the top surface of the semi-magnetic TI is half-quantized when the Fermi energy E_F is tuned the Dirac gap [25]. This coincides with the above analysis.

To investigate the surface transport of a six-terminal Hall-bar device [see Fig. 1(b)], we discretize the Hamiltonian H into $N_x \times N_y \times N_z$ cubic lattice sites. The dephasing process is simulated by using $n_x \times n_y$ and $n_x \times n_z$ Büttiker's virtual leads on the bottom and side surfaces, respectively [25–28]. According to Landauer-Büttiker formula, the current in the lead p can be expressed as:

$$I_p = \frac{e^2}{h} \sum_{q \neq p} (T_{qp} V_p - T_{pq} V_q) \quad (1)$$

where V_p is the voltage in the lead p . $T_{pq}(E_F) = \text{Tr}[\Gamma_p \mathbf{G}^r \Gamma_q \mathbf{G}^a]$ is the transmission coefficient from the lead q to the lead p , where the linewidth function $\Gamma_p = i(\Sigma_p^r - \Sigma_p^i)$ and the Green's function $\mathbf{G}^r = [\mathbf{G}^a]^\dagger = [E_F \mathbf{I} - H_{\text{cen}} - \sum_p \Sigma_p^r]^{-1}$. Σ_p^r is the retarded self-energy due to the coupling to the lead p and H_{cen} is the lattice Hamiltonian of the semi-magnetic TI. For real leads ($p = 1, 2, \dots, 6$), $\Sigma_p^r = -i\frac{\Gamma_p}{2} \mathbf{I}_p$, where \mathbf{I}_p is $4n_p \times 4n_p$ unit matrix and n_p is the number of the sites coupling to the real lead p . For virtual leads, $\Sigma_p^r = -i\frac{\Gamma_v}{2}$, where Γ_v is the dephasing strength [28]. When the longitudinal current I_x flows from lead 1 to 4, the Hall resistance $R_{xy} = (V_2 - V_6)/I_x$ and longitudinal resistance $R_{xx} = (V_2 - V_3)/I_x$ are obtained via Eq. (1). Because the current only flow along the gapless surfaces (two side and one bottom surfaces), one can get $\rho_{xy} = R_{xy}$, and $\rho_{xx} = R_{xx}/(L/W)$. Here, L is the length between lead 2 and 3, and $W = (N_y + 2(N_z - 1) - 1)$ is the total width of the gapless surfaces. The longitudinal and Hall conductance are obtained from the tensor relation: $\sigma_{xx} = \rho_{xx}/(\rho_{xx}^2 + \rho_{xy}^2)$, and $\sigma_{xy} = \rho_{xy}/(\rho_{xx}^2 + \rho_{xy}^2)$.

Now, we show the numerical results of the conductance below. In Fig. 1, the Hall conductance σ_{xy} and the longitudinal conductance σ_{xx} are both non-quantized for a small dephasing strength, e.g. $\Gamma_v = 0.5$. Remarkably, one finds that the Hall conductance σ_{xy} decreases rapidly and arrived at a half-quantized plateau with increasing Γ_v [see Fig. 1(e)], while the longitudinal conductance σ_{xx} remains nonzero [see Fig. 1(f)]. We will explain it later. After this half-quantization, σ_{xy} is independent of Fermi energy E_F [see Figs. 1(c) and (e)]. In addition, σ_{xx} increases almost linearly with E_F in Fig. 1(d) because the density of state of the gapless Dirac cone is proportional to $|E_F|$, and σ_{xx} decreases quickly with increasing Γ_v in Fig. 1(f) due to the momentum relaxation introduced by the virtual leads [29].

Half-quantized chiral channel and HQHC.— To get more insight into the origin of the HQHC, we investigate

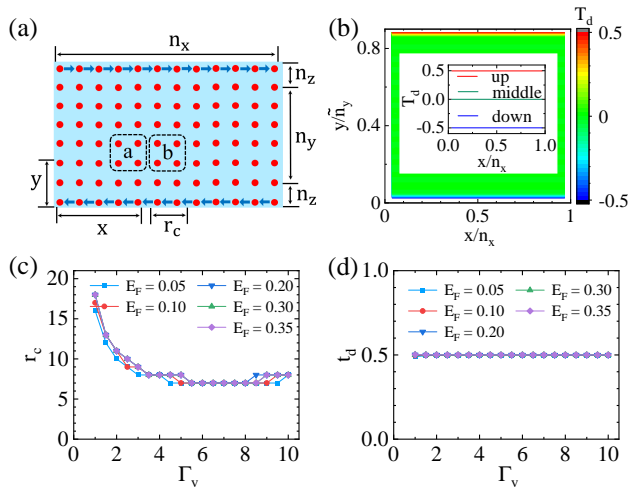


FIG. 2: (Color online). (a) Lay the side and bottom surfaces of the sample in Fig. 1 on the xy plane. The red balls represent the sites attached to virtual leads and the blue arrows indicate chiral edge current. a and b are used to label the black box, and the size of black box is r_c . (x, y) is the coordinate of the red ball in the lower right corner of the box a . (b) The space distribution of the different of transmission coefficients T_d with $\Gamma_v = 4.0$ and $E_F = 0.3$. The inset show the value of T_d in upper edge ($y = \tilde{n}_y - r_c$), middle area ($y = (\tilde{n}_y - r_c)/2$), and the lower edge ($y = 1$). (c) and (d) show r_c and t_d as a function of Γ_v for different E_F . Other parameters are the same as those in Fig. 1.

the transmission coefficients between the virtual leads. For convenience, we lay the side and bottom surfaces on the xy -plane [see Fig. 2(a)]. The red balls represent sites attached to the virtual leads. The total number of virtual leads in the y direction is $\tilde{n}_y = n_y + 2(n_z - 1)$. Numerical results show that the transmission coefficient T_{pq} from lead q to lead p decays sharply with their distance r_{pq} [25]. Thus, we can define a critical distance r_c : $T_{pq} = 0.001T_1$ when $r_{pq} = r_c$, such that T_{pq} can be neglected when $r_{pq} > r_c$. Here, T_1 is the transmission coefficient between two nearest leads. In Fig. 2(c), r_c is proportional to the phase coherent length, and thus decreases with increasing the dephasing strength Γ_v .

In order to reveal the directionality of the transmission, we define the difference of transmission coefficients between black box a and black box b as $T_d(x, y) = T_{ba} - T_{ab}$, where (x, y) is the spatial coordinate of the red ball in the lower right corner of the box a [see Fig. 2(a)]. Here $T_{ba} = \sum_{p \in b, q \in a} T_{pq}$ the transmission coefficient from the box a to the box b , and $p \in a$ means that lead p is in box a [see Fig. 2(a)]. Figure 2(b) shows that $T_d = \pm 1/2$ in the upper edge and the lower edge, respectively, and zero elsewhere. Moreover, $t_d \equiv T_d(n_x/2, \tilde{n}_y - r_c)$, the difference of transmission coefficient near the edges of top surface, keeps half-quantized for different E_F and Γ_v [see Fig. 2(d)]. The half-quantized t_d means that there is a half-quantized chiral channel or a half-quantized chi-

ral current [13] on the edge of the top surface [see the blue arrows in Fig. 2(a)], giving rise to the HQHC. The half-quantized chiral current is rather robust against the dephasing process, so we can obtain a perfect HQHC plateau for different dephasing strengths in Fig. 1(a).

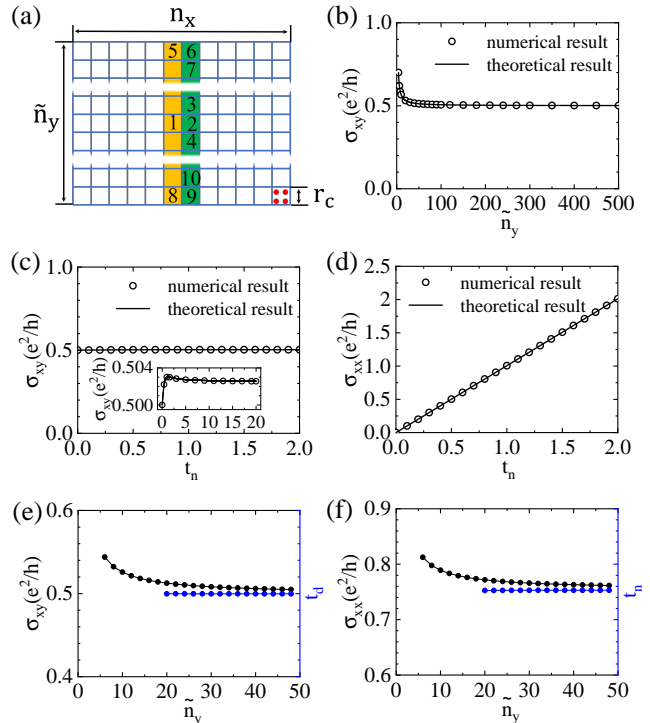


FIG. 3: (Color online). (a) Divide red balls in Fig. 2(a) by using blue boxes, and each blue box contain r_c^2 red balls. The numbers are used to label boxes. (b)-(d) Comparison of the theoretical results and numerical results for a simple case that $r_c = 1$. (b) σ_{xy} as a function of \tilde{n}_y with $t_n = 1$. (c) and (d) σ_{xy} and σ_{xx} as a function of t_n with $\tilde{n}_y = 200$. Other parameters in (b)-(d) are $n_x = 7\tilde{n}_y$ and $t_d = 0.5$. (e) σ_{xy} and t_d as a function of \tilde{n}_y . (f) σ_{xx} and t_n as a function of \tilde{n}_y . The parameters of (e) and (f): $E_F = 0.2$, $\Gamma_v = 3.0$, $n_z = 2$, $n_y = \tilde{n}_y - 2(n_z - 1)$, $n_x = 4\tilde{n}_y$, $N_z = 5$, $N_y = 4(n_y - 1) + 1$, $N_x = 4n_x$, and other parameters are the same as those in Fig. 1.

To establish an analytic relation between σ_{xy} and t_d , we map the system in Fig. 2(a) to a well-studied conductor-network model that describes conduction of a classical metal [30, 31]. Here every r_c^2 red balls in Fig. 2(a) are rearranged into one blue box in Fig. 3(a). Because r_c much larger than the phase coherent length [28], the transmission between two adjacent blue boxes is incoherent, and the system can be regarded as the classical conductor-network model [30, 31]. The conductance of conductor-network model in Fig. 3(a) is determined by the total transmission coefficients between leads in two adjacent blue boxes, since $T_{pq} \ll 1$ when $r_{pq} > r_c$. Using $I_{pq} = (T_{pq}V_q - T_{qp}V_p)$ the current flowing from the lead q

to the lead p , one can get (see more details in Ref. [25]):

$$\begin{aligned}\sigma_{xy} &= \frac{e^2}{h} \left[1 + \frac{r_c \alpha t_n + t_n^2}{t_d^2 + t_n^2} \frac{1}{\tilde{n}_y - 1} \right] t_d \\ \sigma_{xx} &= \frac{e^2}{h} \left[1 + \frac{r_c \alpha t_n + t_n^2}{t_d^2 + t_n^2} \frac{1}{\tilde{n}_y - 1} \right] t_n\end{aligned}\quad (2)$$

where $t_n = t_{12} + t_{13} + t_{14}$ and $\alpha = t_{56} + t_{57} + t_{89} + t_{810} - 2t_n$, with $t_{ij} = \sum_{p \in j, q \in i} T_{pq} x_{pq} / r_c$. $x_{pq} = x_p - x_q$ and $x_p(x_q)$ is the x-coordinate of the lead $p(q)$. $p \in i$ means that lead p is in box i [see Fig. 3(a)]. Notably, in the large size limit when $\tilde{n}_y \gg 1$, we have $\sigma_{xy} = t_d \frac{e^2}{h}$ and $\sigma_{xx} = t_n \frac{e^2}{h}$. This strongly demonstrates that the HQHC is directly related to the existence of half-quantized chiral channel t_d on the edges of the top surface, while σ_{xx} is contributed from the normal channels t_n .

Next, we demonstrate the validity of Eq. (2). First, we consider a simple model with $r_c = 1$, where only the transmission coefficient between two nearest leads is non-zero (see more details in Ref. [25]). In Figs. 3(b-d), we evaluate σ_{xy} and σ_{xx} as a function of t_n and \tilde{n}_y numerically by Eq. (1) and analytically by Eq. (2), respectively, when $t_d = 0.5$. The results are found to be fitting well which justifies Eq.(2). Furthermore, by starting from the realistic semi-magnetic TI Hamiltonian, we calculate σ_{xy} , σ_{xx} , t_n and t_d using Eq. (1) and plot them as a function \tilde{n}_y in Fig. 3(e-f). It is found that σ_{xy} (σ_{xx}) decreases and converges to t_d (t_n) when \tilde{n}_y increasing, which is coincident with the theoretical results of Eq. (2) and thus again confirm the validity of Eq. (2). This strongly demonstrates the consistency and reliability of the obtained results. In realistic systems, if \tilde{n}_y or Γ_v is too small so that $\tilde{n}_y / r_c \lesssim 1$, the half-quantized chiral current on the upper and lower edges will spatially mix due to finite t_n , which sabotages the quantization of σ_{xy} . Therefore, we conclude that the dephasing process plays a key role in the separation of the two half-quantized chiral current in a metallic region, thus giving rise to the HQHC. This mechanism of the HQHC is very different from that of the conventional quantized Hall conductance which is observed in an insulating phase [5].

Comparison with experimental transport results– Recently, the Hall conductance σ_{xy} is experimentally reported to be half-quantized in the semi-magnetic TI [22]. In contrast, the Hall resistance ρ_{xy} and longitudinal resistance ρ_{xx} that directly measured in the experiments, as well as the longitudinal conductance σ_{xx} , are all non-quantized. Further, they show the temperature dependence of ρ_{xx} , ρ_{xy} , σ_{xx} and σ_{xy} . As a comparison, we calculate ρ_{xx} , ρ_{xy} , σ_{xx} and σ_{xy} as a function of T by using Landauer-Büttiker formula at non-zero temperature [32]: $I_p = \frac{e^2}{h} \sum_{q \neq p} (\tilde{T}_{qp} V_p - \tilde{T}_{pq} V_q)$. Here $\tilde{T}_{pq}(T, E_F) = \int T_{pq}(E) (-\frac{\partial f_0}{\partial E}) dE$ with the Fermi distribution $f_0 = [e^{(E-E_F)/k_B T} + 1]^{-1}$ and the Boltzmann constant k_B .

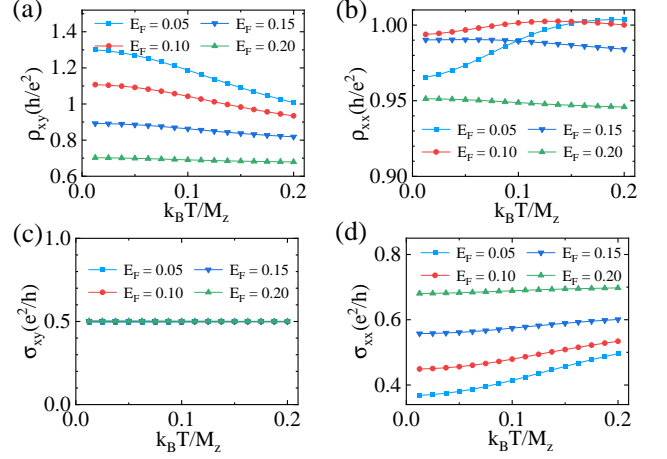


FIG. 4: (Color online). Hall resistance ρ_{xy} (a), longitudinal resistance ρ_{xx} (b), Hall conductance σ_{xy} (c) and longitudinal conductance σ_{xx} (d) as a function of temperature T . The curves correspond to different Fermi energy E_F . The dephasing strength $\Gamma_v = 4.0$, and other parameters are the same as those in Fig. 1.

In Figs. 4(a-b), both ρ_{xx} and ρ_{xy} are non-quantized and vary with T and E_F . Remarkably, when the resistance [in Figs. 4(a-b)] is converted into the conductance, σ_{xy} is half-quantized and σ_{xx} is a monotonically increasing function of T for different E_F [see Figs. 4(c-d)], which is utterly consistent with the experimental results. Based on the Landauer-Büttiker formula at non-zero temperature, one gets $\sigma_{xy}(E_F, T) = \int \sigma_{xy}(E, T=0) (-\frac{\partial f_0}{\partial E}) dE$ and $\sigma_{xx}(E_F, T) = \int \sigma_{xx}(E, T=0) (-\frac{\partial f_0}{\partial E}) dE$ for $\tilde{n}_y \gg 1$ [25]. This indicates that the dependence of conductance on the Fermi energy at zero temperature, determines the temperature dependence of conductance. In Fig. 4(d), σ_{xx} increases with T because σ_{xx} increases almost linearly with $|E_F|$ at zero temperature, while σ_{xy} is independent of T in Fig. 4(c) because σ_{xy} is independent of E_F at zero temperature. Then, ρ_{xy} decreases with T since $\rho_{xy} = \sigma_{xy} / (\sigma_{xx}^2 + \sigma_{xy}^2)$ is a monotonically decreasing function of σ_{xx} . $\rho_{xx} = \sigma_{xx} / (\sigma_{xx}^2 + \sigma_{xy}^2)$ increases with σ_{xx} for $\sigma_{xx} < \sigma_{xy}$ and decreases with σ_{xx} for $\sigma_{xx} > \sigma_{xy}$. So ρ_{xx} will increase first and then decrease with T since $\sigma_{xx} < \sigma_{xy}$ at zero temperature for $E_F = 0.05$ and 0.10 , and monotonically decreases with T since $\sigma_{xx} > \sigma_{xy}$ at zero temperature for $E_F = 0.15$ and 0.20 .

Conclusion and discussion– In summary, we reveal that the half-quantized chiral current along the edge of a strongly dephasing metal is the origin of the HQHC of the semi-magnetic TI. In reality, a 2D metal should be strongly influenced by the disorder, and the gapless Dirac cone could be driven into a critical metallic phase that can also host the HQHC [18, 19]. Nevertheless, the HQHC is measured in a hundreds-micron sample in the experiment, which far exceeds the dephasing length, and thus the system belongs to a classical metal.

Acknowledgement.— We thank M. Mogi, Jing-Yun Fang, Junjie Qi, Haiwen Liu and Hua Jiang for illuminating discussions. This work was financially supported by National Key R and D Program of China (Grant No. 2017YFA0303301), NBRPC (Grant No. 2015CB921102), NSFC (Grants Nos. 11534001, 11822407, 11921005, 12074108, and 11704106), and also supported by the Fundamental Research Funds for the Central Universities, the Strategic Priority Research Program of Chinese Academy of Sciences (DB28000000), and Beijing Municipal Science & Technology Commission (Grant No. Z191100007219013). C.-Z.C. is also funded by the Priority Academic Program Development of Jiangsu Higher Education Institutions.

* Electronic address: czchen@suda.edu.cn

† Electronic address: xcxie@pku.edu.cn

- [1] A. J. Niemi and G. W. Semenoff, *Phys. Rev. Lett.* **51**, 2077 (1983).
- [2] R. Jackiw, *Phys. Rev. D* **29**, 2375 (1984).
- [3] G. W. Semenoff, *Phys. Rev. Lett.* **53**, 2449 (1984).
- [4] E. Fradkin, E. Dagotto, and D. Boyanovsky, *Phys. Rev. Lett.* **57**, 2967 (1986).
- [5] F. D. M. Haldane, *Phys. Rev. Lett.* **61**, 2015 (1988).
- [6] L. Fu, C. L. Kane, and E. J. Mele, *Phys. Rev. Lett.* **98**, 106803 (2007).
- [7] L. Fu and C. L. Kane, *Phys. Rev. B* **76**, 045302 (2007).
- [8] A. H. Castro Neto, F. Guinea, N. M. R. Peres, K. S. Novoselov, and A. K. Geim, *Rev. Mod. Phys.* **81**, 109 (2009).
- [9] X.-L. Qi and S.-C. Zhang, *Rev. Mod. Phys.* **83**, 1057 (2011).
- [10] X.-L. Qi, T. L. Hughes, and S.-C. Zhang, *Phys. Rev. B* **78**, 195424 (2008).
- [11] K. Nomura and N. Nagaosa, *Phys. Rev. Lett.* **106**, 166802 (2011).
- [12] Y. D. Lensky, J. C. W. Song, P. Samutpraphoot, and L. S. Levitov, *Phys. Rev. Lett.* **114**, 256601 (2015).
- [13] R.-L. Chu, J. Shi, and S.-Q. Shen, *Phys. Rev. B* **84**, 085312 (2011).
- [14] E. J. König, P. M. Ostrovsky, I. V. Protodopov, I. V. Gornyi, I. S. Burmistrov, and A. D. Mirlin, *Phys. Rev. B* **90**, 165435 (2014).
- [15] R. Yoshimi, K. Yasuda, A. Tsukazaki, K. S. Takahashi, N. Nagaosa, M. Kawasaki, and Y. Tokura, *Nature communications* **6**, 1 (2015).
- [16] K. S. Novoselov, A. K. Geim, S. V. Morozov, D. Jiang, M. I. Katsnelson, I. V. Grigorieva, S. V. Dubonos, and A. A. Firsov, *Nature* **438**, 197 (2005).
- [17] Y. Zhang, Y.-W. Tan, H. L. Stormer, and P. Kim, *Nature* **438**, 201 (2005).
- [18] M. Mogi, M. Kawamura, R. Yoshimi, A. Tsukazaki, Y. Kozuka, N. Shirakawa, K. S. Takahashi, M. Kawasaki, and Y. Tokura, *Nat. Mater.* **16**, 516 (2017).
- [19] D. Xiao, J. Jiang, J.-H. Shin, W. Wang, F. Wang, Y.-F. Zhao, C. Liu, W. Wu, M. H. W. Chan, N. Samarth, and C.-Z. Chang, *Phys. Rev. Lett.* **120**, 056801 (2018).
- [20] R. Lu, H. Sun, S. Kumar, Y. Wang, M. Gu, M. Zeng, Y.-J. Hao, J. Li, J. Shao, X.-M. Ma, Z. Hao, K. Zhang, W. Mansuer, J. Mei, Y. Zhao, C. Liu, K. Deng, W. Huang, B. Shen, K. Shimada, E. F. Schwier, C. Liu, Q. Liu, and C. Chen, *Phys. Rev. X* **11**, 011039 (2021).
- [21] H. Nielsen and M. Ninomiya, *Nuclear Physics B* **185**, 20 (1981).
- [22] M. Mogi, Y. Okamura, M. Kawamura, R. Yoshimi, K. Yasuda, A. Tsukazaki, K. S. Takahashi, T. Morimoto, N. Nagaosa, M. Kawasaki, Y. Takahashi, and Y. Tokura, *Nature Physics* (2022).
- [23] E. Prodan, *Phys. Rev. B* **80**, 125327 (2009).
- [24] E. Prodan, *Journal of Physics A: Mathematical and Theoretical* **44**, 239601 (2011).
- [25] “See supplemental material for detailed discussions about a real-space kubo formula calculation, the lattice model hamiltonian, the expressions of conductance at zero temperature and low temperature, and transmission coefficients of the simple model,” .
- [26] M. Büttiker, *Phys. Rev. Lett.* **57**, 1761 (1986).
- [27] M. Büttiker, *IBM Journal of Research and Development* **32**, 317 (1988).
- [28] Y. Xing, Q.-f. Sun, and J. Wang, *Phys. Rev. B* **77**, 115346 (2008).
- [29] R. Golizadeh-Mojarad and S. Datta, *Phys. Rev. B* **75**, 081301 (2007).
- [30] S. Kirkpatrick, *Phys. Rev. Lett.* **27**, 1722 (1971).
- [31] P. Erdős and S. B. Haley, *Phys. Rev. B* **13**, 1720 (1976).
- [32] S. Datta, *Electronic Transport in Mesoscopic Systems* (Cambridge University Press, Cambridge, 1995).

Supplementary Materials for “Transport Theory of Half-quantized Hall Conductance in a Semi-magnetic Topological Insulator”

Humian Zhou,¹ Hailong Li,¹ Dong-Hui Xu,² Chui-Zhen Chen,^{3,4,*} Qing-Feng Sun,^{1,5,6} and X. C. Xie^{1,5,6,†}

¹International Center for Quantum Materials, School of Physics, Peking University, Beijing 100871, China

²Department of Physics, Chongqing University, Chongqing 400044, China

³School of Physical Science and Technology, Soochow University, Suzhou 215006, China

⁴Institute for Advanced Study, Soochow University, Suzhou 215006, China

⁵Collaborative Innovation Center of Quantum Matter, Beijing 100871, China

⁶CAS Center for Excellence in Topological Quantum Computation, University of Chinese Academy of Sciences, Beijing 100190, China

(Dated: February 1, 2022)

CONTENTS

S1. Layer-dependent Hall conductance of semi-magnetic topological insulator	S1
S2. Lattice model Hamiltonian and dephasing	S2
S3. Derivation of the expressions of conductance at zero temperature	S2
S4. Transmission coefficients of the simple model	S4
S5. Conductance at non-zero temperature	S4
References	S5

S1. LAYER-DEPENDENT HALL CONDUCTANCE OF SEMI-MAGNETIC TOPOLOGICAL INSULATOR

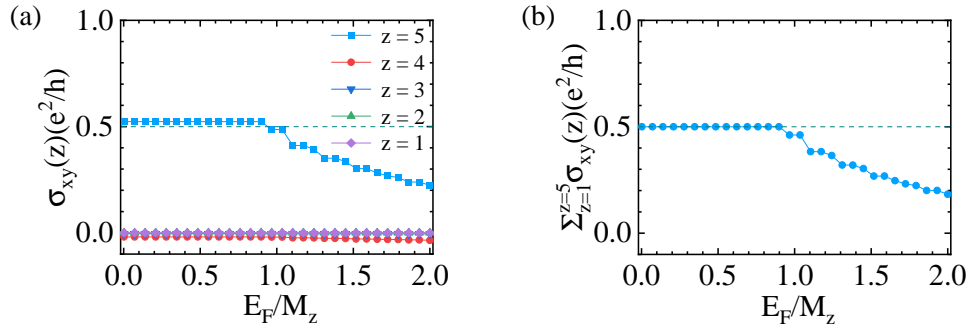


FIG. S1. (a) The layer-dependent Hall conductance $\sigma_{xy}(z)$ as a function of Fermi energy E_F . z is the layer index with $z = 1$ for the bottom layer and $z = 5$ for the top layer. (b) The total Hall conductance as a function of E_F . Here, the size of sample is $N_x \times N_y \times N_z = 40 \times 40 \times 5$. Other parameters are $A = 1.0$, $B = 0.6$, $M_0 = 1.0$ and $M_z = 0.4$.

In this section, we calculate the layer-dependent Hall conductance of semi-magnetic topological insulator (TI) by the real-space Kubo formula[1, 2]

$$\sigma_{xy}(z) = \frac{2\pi i e^2}{h} \text{Tr} \{P[-i[\hat{x}, P], -i[\hat{y}, P]]\}_z \quad (1)$$

* czchen@suda.edu.cn

† xcxie@pku.edu.cn

with periodic boundary condition in both the x and y direction. (\hat{x}, \hat{y}) denotes the position operator, and $\text{Tr}\{\dots\}_z$ is trace over the wave functions of the z th layer. P is the projector onto the occupied states of the effective Hamiltonian H of the semi-magnetic TI. Figure S1(a-b) plots the layer-dependent Hall conductance $\sigma_{xy}(z)$ and the total conductance $\sum_{z=1}^5 \sigma_{xy}(z)$ as a function of Fermi energy E_F , respectively. As E_F is located in the Dirac gap, the total Hall conductance is half-quantized and the non-zero Hall conductance is mainly from the top surface.

S2. LATTICE MODEL HAMILTONIAN AND DEPHASING

We discretize the Hamiltonian H in the main text on cubic lattices:

$$H = \left[\sum_{\mathbf{i}} \mathbf{c}_{\mathbf{i}}^{\dagger} \mathcal{M}_0 \mathbf{c}_{\mathbf{i}} + \left(\sum_{\mathbf{i}, j=x,y,z} \mathbf{c}_{\mathbf{i}}^{\dagger} \mathcal{T}_j \mathbf{c}_{\mathbf{i}+\hat{\mathbf{e}}_j} + \text{H.c.} \right) \right] + \sum_{\mathbf{i} \in \text{top surface}} \mathbf{c}_{\mathbf{i}}^{\dagger} \mathcal{M}_z \mathbf{c}_{\mathbf{i}} + H_d \quad (2)$$

where $\mathcal{M}_0 = (M_0 - 6B/a^2) \sigma_z \otimes s_0$, $\mathcal{M}_z = M_z \sigma_0 \otimes s_z$, and $\mathcal{T}_j = B/a^2 \sigma_z \otimes s_0 - iA/(2a) \sigma_x \otimes s_j$. Here, $a = 1$ is the cubic lattice constant. $\mathbf{c}_{\mathbf{i}}$ ($\mathbf{c}_{\mathbf{i}}^{\dagger}$) is the annihilation (creation) operator at site \mathbf{i} , and $\hat{\mathbf{e}}_j$ is a unit vector in the j direction for $j = x, y, z$. The first and the second terms in Eq. (2) describe the semi-magnetic topological insulator (TI) in the central region. The last term $H_d = \sum_{\mathbf{i}, \mathbf{k}} \left[\epsilon_{\mathbf{k}} \mathbf{a}_{\mathbf{i}, \mathbf{k}}^{\dagger} \mathbf{a}_{\mathbf{i}, \mathbf{k}} + (t_{\mathbf{i}, \mathbf{k}} \mathbf{a}_{\mathbf{i}, \mathbf{k}}^{\dagger} \mathbf{c}_{\mathbf{i}} + \text{H.c.}) \right]$ represents the Hamiltonian of virtual leads and real leads, and their couplings to the central sites. Note that we use the wide-band approximation for the real leads in the main text with parameters $\Gamma_1 = \Gamma_4 = 0.9$, $n_1 = n_4 = N_z \times N_y$, $\Gamma_i = \Gamma_v$ and $n_i = n_z$ for $i = 2, 3, 5, 6$, where Γ_v is the dephasing strength. Only electrons in the gapless surface states participate in the electrical transport when E_F is located in the Dirac gap at zero or low temperature. Therefore, we just need to consider the dephasing process on the side and bottom surfaces. We simulate the dephasing process by using $n_x \times n_y$ uniformly distributed Büttiker's virtual leads on the bottom surface and $n_x \times n_z$ uniformly distributed Büttiker's virtual leads on each side surface. N_i and n_i are the number of total sites and selected sites in the i direction for $i = x, y, z$, respectively.

In our calculations, real lead 1 and 4 act as current electrodes and other real leads act as voltage electrodes. Thus, the longitudinal current $I_1 = -I_4 \equiv I_x$ when an external bias is applied between lead 1 and lead 4 with $V_1 = V/2$ and $V_4 = -V/2$. Virtual leads act as dephasing, so the net current of each virtual lead is zero. Combining Landauer-Büttiker formula [3, 4] with those boundary conditions in the real and virtual leads, one can calculate the voltage of each real lead and the longitudinal current I_x . Then the Hall resistance $R_{xy} = (V_2 - V_6)/I_x$ and longitudinal resistance $R_{xx} = (V_2 - V_3)/I_x$ will be obtained.

S3. DERIVATION OF THE EXPRESSIONS OF CONDUCTANCE AT ZERO TEMPERATURE

In this section, we explain in detail how to derive the expressions of the Hall and longitudinal conductance. We lay the two side surfaces and the bottom surface of sample on the xy -plane, and divide red balls by blue boxes. Red balls represent sites attached virtual leads, so each blue box contains r_c^2 red balls [see Fig. S2(a)]. Before derivation, let us discuss about three important assumptions and their validity.

Firstly, we discuss about the critical length r_c . Fig. S2(b) plot the transmission coefficient T_{pq} from virtual lead q to virtual lead p versus their distance r_{pq} . T_1 is the transmission coefficient between two nearest leads. The results show that T_{pq} decreases sharply with increasing r_{pq} . We define a critical distance r_c satisfying that $T_{pq} = 0.001T_1$ when $r_{pq} = r_c$. Thus T_{pq} can be neglected when $r_{pq} > r_c$, which is the first assumption.

Secondly, we define longitudinal and transverse electric field as: $E_x \equiv V_q - V_{q+\hat{\mathbf{e}}_x} > 0$, $E_y \equiv V_{q+\hat{\mathbf{e}}_y} - V_q > 0$. Here, V_q and $V_{q+\hat{\mathbf{e}}_x}$ are the voltages of the lead p and its nearest lead on the x direction, respectively. The numerical results demonstrate that the electric field is almost constant in the middle area of the gapless surface although it changes when closing to the real lead 1 and lead 4. Therefore, the electric field of the green area and orange area can be thought to be constant, which is the second assumption.

The last assumption is that the difference of transmission coefficient between two nearest boxes is non-zero in the upper edge and lower edge, which is verified by numerical results of Fig. 2(b) in the main text.

Because T_{pq} is so small that it can be neglected when $r_{pq} > r_c$, only the current I_{pq} of two leads within one blue box or separately in two adjacent blue boxes is non-zero according to Landauer-Büttiker formula [3, 4]. $I_{pq} = e^2/h(T_{pq}V_q - T_{qp}V_p)$ is the net current flowing from lead q to lead p . Then, one can get the total current flowing

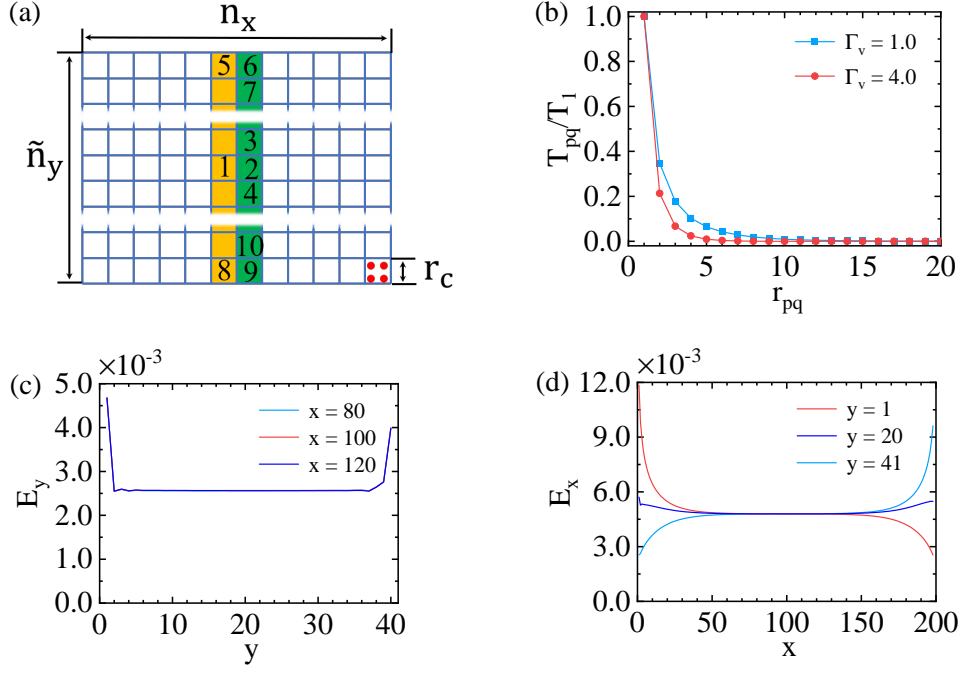


FIG. S2. (color online) (a) Divide red balls in Fig.2.(a) in the main text by using blue boxes, and each blue box contain r_c^2 red balls. The numbers are used to label boxes. (b) T_{pq}/T_1 vs r_{pq} for different Γ_v with $E_F = 0.3$. T_{pq} is the transmission coefficient from virtual lead q to virtual lead p , and r_{pq} is the distance of those two leads. T_1 is the transmission coefficient between two nearest leads. (c) and (d) E_x vs x for different y and E_y vs y for different x . (E_x, E_y) is the electric field and (x, y) is the coordinate of red balls. $\Gamma_v = 4.0$ and $E_F = 0.3$ in (c) and (d). Here, $N_x = 800$, $N_y = 153$, $N_z = 5$, $n_x = 200$, $n_y = 39$, $n_z = 2$, and $\tilde{n}_y = 41$. Other parameters are $A = 1.0$, $B = 0.6$, $M_0 = 1.0$ and $M_z = 0.4$.

in the horizontal (x) direction:

$$\begin{aligned}
 I_x &= \sum_{p \in g, q \in o} I_{pq} = \sum_{p \in g, q \in o} (T_{pq}V_q - T_{qp}V_p) \\
 &= \sum_{p \in g, q \in o} T_{pq}(V_q - V_p) + \sum_{p \in g, q \in o} (T_{pq} - T_{qp})V_p \\
 &= \sum_{p \in g, q \in o} T_{pq}(x_{pq}E_x + y_{qp}E_y) + \sum_{p \in 6, q \in 5} (T_{pq} - T_{qp})V_p + \sum_{p \in 9, q \in 8} (T_{pq} - T_{qp})V_p \\
 &= (t_n \tilde{n}_y + r_c \alpha)E_x + t_d V_u - t_d V_d \\
 &= t_n E_x \tilde{n}_y + r_c \alpha E_x + t_d E_y (\tilde{n}_y - 1)
 \end{aligned} \tag{3}$$

Where the V_u (V_d) is the voltage of the upper (lower) edge, and $V_u - V_d = E_y(\tilde{n}_y - 1)$. $p(q) \in g(o)$ means that lead $p(q)$ is in the green (orange) area [see Fig. S2(a)]. Here, we have assumed T_{pq} to be translational invariant on the gapless surface apart from its edges. The first term of I_x is the normal current, and the third term is the current from Hall effect. The second term is the extra current from the difference between the conductance in the gapless surface and the conductance at its edge. Here, $t_n = t_{12} + t_{13} + t_{14}$ and $\alpha = t_{56} + t_{57} + t_{89} + t_{810} - 2t_n$. $t_{ij} = \sum_{p \in j, q \in i} T_{pq} x_{pq} / r_c$. $x_{pq} = x_p - x_q$ and $x_{p(q)}$ is the x-coordinate of the lead $p(q)$. $p \in i$ means that lead p is in box i [see Fig. S2(a)]. And t_n is isotropic and constant on the gapless surface (not include the edges of the surface). Similarly, one can get the current flowing in the vertical (y) direction $I_y = t_n E_y n_x + r_c \alpha E_y - t_d E_x (n_x - 1)$. In our real model, $n_x \gg 1$ and $I_y = 0$, thus $t_n E_y = t_d E_x$. Then $\rho_{xx} = E_x(\tilde{n}_y - 1)/I_x$ and $\rho_{xy} = E_y(\tilde{n}_y - 1)/I_x$. By converting the resistance to the conductance, one can get:

$$\sigma_{xy}(E_F) = \frac{e^2}{h} \left[1 + \frac{r_c \alpha t_n + t_n^2}{t_d^2 + t_n^2} \frac{1}{\tilde{n}_y - 1} \right] t_d \tag{4}$$

$$\sigma_{xx}(E_F) = \frac{e^2}{h} \left[1 + \frac{r_c \alpha t_n + t_n^2}{t_d^2 + t_n^2} \frac{1}{\tilde{n}_y - 1} \right] t_n \tag{5}$$

S4. TRANSMISSION COEFFICIENTS OF THE SIMPLE MODEL

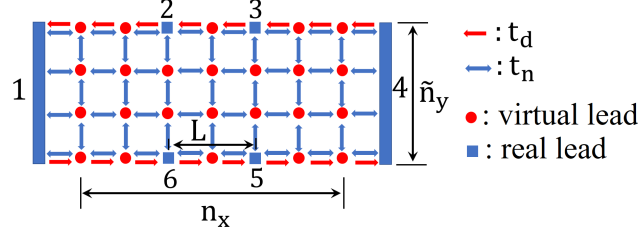


FIG. S3. (color online) Schematic plot of the transmission coefficients of the simple model. The blue square and rectangle represent the real lead while the red circle represents the virtual lead. The double blue arrow indicate $T_{pq} = T_{qp} = t_n$ for two nearest leads. The single red arrow indicate an extra transmission t_d coefficient from one lead to another lead that the red single arrow points to.

In this section, we will illustrate the transmission coefficients of leads in the simple model with $r_c = 1$. For this simple model, only the transmission coefficient between two nearest leads is non-zero. As shown in Fig. S3, $T_{p,q} = T_{q,p} = t_n$ for two nearest leads (include real leads and virtual leads). Considering the difference of transmission coefficients is non-zero in the edge, we have $T_{p+\hat{e}_x,p} = t_n$ and $T_{p,p+\hat{e}_x} = t_n + t_d$ in the upper edge, and $T_{p+\hat{e}_x,p} = t_n + t_d$ and $T_{p,p+\hat{e}_x} = t_n$ in the lower edge. Here, $p + \hat{e}_x$ represents the lead on the right-hand of lead p . Obviously, $\alpha = t_d$. The width of the sample is $W = \tilde{n}_y - 1$, and the distance between real lead 2 and lead 3 is $L = W$. Given the transmission coefficients of leads, σ_{xy} and σ_{xx} can be calculated numerically by Landauer-Büttiker formula and then compared to Eqs.(4-5).

S5. CONDUCTANCE AT NON-ZERO TEMPERATURE

In this section, we derive the Hall and longitudinal conductance at low temperature. In our numerical simulations, we use the Landauer-Büttiker formula at non-zero temperature[4]:

$$I_p = \frac{e^2}{h} \sum_{q \neq p} \left(\tilde{T}_{qp}(T, E_F) V_p - \tilde{T}_{pq}(T, E_F) V_q \right) \quad (6)$$

Here, $\tilde{T}_{pq}(T, E_F) = \int T_{pq}(E) \left(-\frac{\partial f_0}{\partial E} \right) dE$. $f_0 = [e^{(E-E_F)/k_B T} + 1]^{-1}$ is the Fermi distribution function, E_F is the Fermi energy, and k_B is the Boltzmann constant. In the section S3, we obtain the expression of conductance. Here, Similarly, one can get the total current flowing in the horizontal (x) direction $I_x = \tilde{t}_n E_x \tilde{n}_y + \tilde{\alpha} E_x + \tilde{t}_d E_y (\tilde{n}_y - 1)$ and the relation $\tilde{t}_n E_y = \tilde{t}_d E_x$ since the total current flowing in the vertical (y) direction $I_y = \tilde{t}_n E_y n_x - \tilde{t}_d E_x (n_x - 1) = 0$ with $n_x \gg 1$. Here, $\tilde{t}_n(T, E_F) = \int t_n(E) \left(-\frac{\partial f_0}{\partial E} \right) dE$, $\tilde{t}_d(T, E_F) = \int t_d(E) \left(-\frac{\partial f_0}{\partial E} \right) dE$ and $\tilde{\alpha}(T, E_F) = \int \alpha(E) r_c(E) \left(-\frac{\partial f_0}{\partial E} \right) dE$. Then, one gets:

$$\sigma_{xy}(E_F, T) = \frac{e^2}{h} \left[1 + \frac{\tilde{\alpha} \tilde{t}_n + (\tilde{t}_n)^2}{(\tilde{t}_d)^2 + (\tilde{t}_n)^2} \frac{1}{\tilde{n}_y - 1} \right] \tilde{t}_d \quad (7)$$

$$\sigma_{xx}(E_F, T) = \frac{e^2}{h} \left[1 + \frac{\tilde{\alpha} \tilde{t}_n + (\tilde{t}_n)^2}{(\tilde{t}_d)^2 + (\tilde{t}_n)^2} \frac{1}{\tilde{n}_y - 1} \right] \tilde{t}_n \quad (8)$$

When $n_y \gg 1$, $\sigma_{xy}(E_F, T) = \tilde{t}_d$ and the expression in Eq.4 $\sigma_{xy}(E, T = 0) = t_d(E)$. Then, one gets:

$$\sigma_{xy}(E_F, T) = \int \sigma_{xy}(E, T = 0) \left(-\frac{\partial f_0}{\partial E} \right) dE \quad (9)$$

Similarly,

$$\sigma_{xx}(E_F, T) = \int \sigma_{xx}(E, T = 0) \left(-\frac{\partial f_0}{\partial E} \right) dE \quad (10)$$

Here, $\sigma_{xy}(E, T = 0)$ and $\sigma_{xx}(E, T = 0)$ are the Hall and longitudinal conductance at zero temperature, respectively[see Eq.4 and 5]. Eq.9 and 10 means that the total conductance comes from the carriers with energy near Fermi energy (that is, $E_F - (\text{a few } k_B T) < E < E_F + (\text{a few } k_B T)$). Moreover, the dependence of conductance on the Fermi energy at zero temperature, determines the temperature dependence of conductance.

In the semi-magnetic TI, the Hall conductance at zero temperature $\sigma_{xy}(E, T = 0)$ is independent of E [see Fig.1(c) in the main text]. Then $\sigma_{xy}(E_F, T) = \sigma_{xy}(E_F, T = 0) = 0.5$ according to the Eq.9, which is why $\sigma_{xy}(E_F, T)$ is half-quantized and independent of temperature in our numerical results and the experimental results. The longitudinal conductance $\sigma_{xx} \propto |E_F|$ due to the gapless Dirac cone[see Fig.1(d) in the main text]. Given $\sigma_{xx}(E, T = 0) = c|E|$, and combine with the Eq.10, one gets:

$$\frac{\sigma_{xx}(E_F, T)}{\sigma_{xx}(E_F, T = 0)} = 1 + \frac{2k_B T}{|E_F|} \ln(1 + e^{-|E_F|/(k_B T)}) \quad (11)$$

Obviously, $\sigma_{xx}(E_F, T)$ is a monotonically increasing function of T , which coincides with our numerical results and the experimental results. Actually, only carriers with energy near Fermi energy (that is, $E_F - (\text{a few } k_B T) < E < E_F + (\text{a few } k_B T)$) have contributions to the longitudinal conductance. When $E_F > 0$, holes with energy below Dirac point contribute to the extra conductance (the second term in Eq.11), making the total conductance at low temperature larger than that at zero temperature. When the temperature is higher, or the Fermi energy is more close to the Dirac point, the number of holes participating in electric transport is more. Therefore, $\sigma_{xx}(E_F, T)$ is a monotonically increasing function of T , and increases faster as the Fermi energy is more close to the Dirac point.

-
- [1] E. Prodan, *Phys. Rev. B* **80**, 125327 (2009).
 - [2] E. Prodan, *Journal of Physics A: Mathematical and Theoretical* **44**, 239601 (2011).
 - [3] M. Büttiker, *IBM Journal of Research and Development* **32**, 317 (1988).
 - [4] S. Datta, *Electronic Transport in Mesoscopic Systems* (Cambridge University Press, Cambridge, 1995).